Supporting Information for

Benzoyl Halides as Alternative Precursors for the Colloidal Synthesis of Lead Based Halide Perovskite Nanocrystals

Muhammad Imran[a,b], Vincenzo Caligiuri[a], Mengjiao Wang[a,b], Luca Goldoni[c,d], Mirko Prato[e], Roman Krahne[a], Luca De Trizio*[a] and Liberato Manna*[a]

[a]Nanochemistry Department, [c]D3 PharmaChemistry Line Department, [d]Analytical Chemistry Facility and [e]Materials Characterization Facility, Istituto Italiano di Tecnologia (IIT), via Morego 30, Genova, Italy

[b]Dipartimento di Chimica e Chimica Industriale, Università degli Studi di Genova, Via Dodecaneso 31, 16146 Genova, Italy

Nuclear Magnetic Resonance (NMR).

NMR analyses were performed on pure benzoyl chloride, benzoic acid, and benzoyl iodide which was prepared by reacting benzoyl chloride with sodium iodide (see the Experimental details in the main text and Figure S1). The benzoic acid was purchased (99.5% purity) from Sigma Aldrich. The compounds were all diluted with toluene-d8 (0.5ml), to a final concentration of 0.1M, before NMR analysis. All spectra were acquired on a Bruker Avance III 400 MHz spectrometer, which was equipped with a Broad Band Inverse probe (BBI). Before each acquisition, automatic matching and tuning were performed, the temperature was actively controlled at 300K, the 90° pulse was optimized by an automatic pulse calculation routine.[1]

^{1}H-*q*NMR (*quantitative NMR*): 16 transients were accumulated, without steady state scans, over a spectral width of 20.55 ppm (offset at 6.175 ppm), at a fixed receiver gain (1), using 30 s of inter pulse delays.

^{13}C-NMR: 5632 transients were accumulated after a 30 degree pulse and 4 steady state scans, over a spectral width of 239 ppm (offset at 100 ppm), using 5 s of inter pulse delays. The receiver gain was automatically adjusted.

2D NMR experiments were acquired as follows (spectra not reported):

^{1}H-^{13}C HSQC (multiplicity edited Heteronuclear Single Quantum Coherence): 2 FIDs, 1024 data points, 256 increments, ^{1}JCH = 145 Hz, spectral width of 7.4 ppm for ^{1}H and 165 ppm for ^{13}C (offsets at 5.08 and 75 ppm, respectively).

^{1}H-^{13}C HMBC (Heteronuclear Multiple Bond Correlation): 16 FIDs, 512 data points, 128 increments, ^{1}JCH long range = 8Hz, spectral width of 13 ppm for ^{1}H and 222 ppm for ^{13}C (offsets at 5 and 100 ppm, respectively).

All NMR chemical shifts refer to the toluene not deuterated residue peak at 2.09 ppm and 20.4 ppm, at ^{1}H-NMR and ^{13}C-NMR respectively.

NMR assignment of chemical species in reaction mixture in toluene-d8

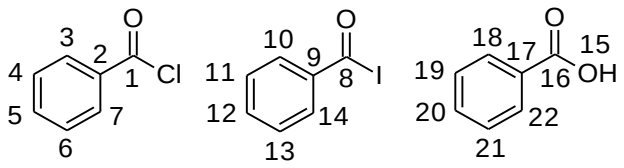

Assignment	^{1}H	*J*(Hz)		^{13}C
15	13.26	-	*br s*	-
18, 22	8.05	-	*m*	130.5
3, 7	7.75	9.9, 8.6	*dd*	131.4
10, 14	7.56	9.6, 8,3	*dd*	132.3
20	7.12	-	*m*	133.7
19, 21	7.02	-	*m*	128.5
5	6.99	-	*m*	134.9
12	6.94	7.43	*br t*	135.1
4, 6	6.82	-	*m*	128.8
11, 13	6.74	-	*m*	128.6
16	-	-	CO	173.1
1	-	-	CO	167.8
8	-	-	CO	159.5
2	-	-	C	133.5
9	-	-	C	137.2
17	-	-	C	129.8

Identification of species in solution. The shielding effect (shift to high field) on the resonances of the protons in position ortho to the acylic group was observed as a consequence of the substitution of the chlorine (see Figure S1A *i*, 3 and 7) with the iodine (see Figure S1A *ii*, 10 and 14), due to the lower electronegativity of iodine compared to that of chlorine. An analogous shift to the high field was observed for the ^{13}C resonances of the CO groups (**8** with respect to **1**), while a shift to the low field was ascertained for the ^{13}C resonance of the α-carbon (**9** compared to **2)** after the substitution of the chlorine with the iodine (see Figure S1B *i* and *ii*).

Reaction yield. The reaction yield, which was measured by a *quantitative* NMR (*q*NMR), is virtually complete (97.7%, with only 2.3% of residual benzoyl chloride). A small amount of benzoic acid (1.2%), which was unambiguously identified by using an authentic material (see Figure S2 A iii and B iii), likely derives from the traces of moisture in the reactants or is due to the cap of the NMR tube not being sealed during the analysis. Indeed, over time, repeated analyses show an increase in the intensity of the benzoic acid signals, which are accompanied by a corresponding reduction in the intensity of the signals of the benzoyl iodide. The high reactivity with water is a further confirmation of the chlorine substitution with the iodine.

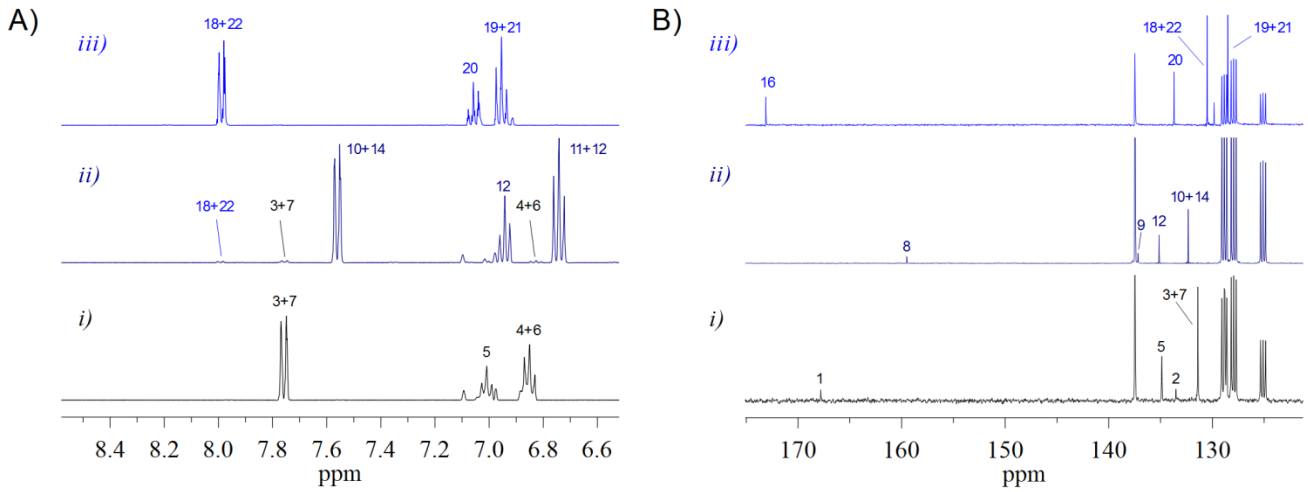

Figure S1. (A) ^{1}H NMR spectra of i) benzoyl chloride, ii) benzoyl iodide, iii) benzoic acid; (B) ^{13}C NMR spectra of i) benzoyl chloride, ii) benzoyl iodide, iii) benzoic acid, in toluene-d8.

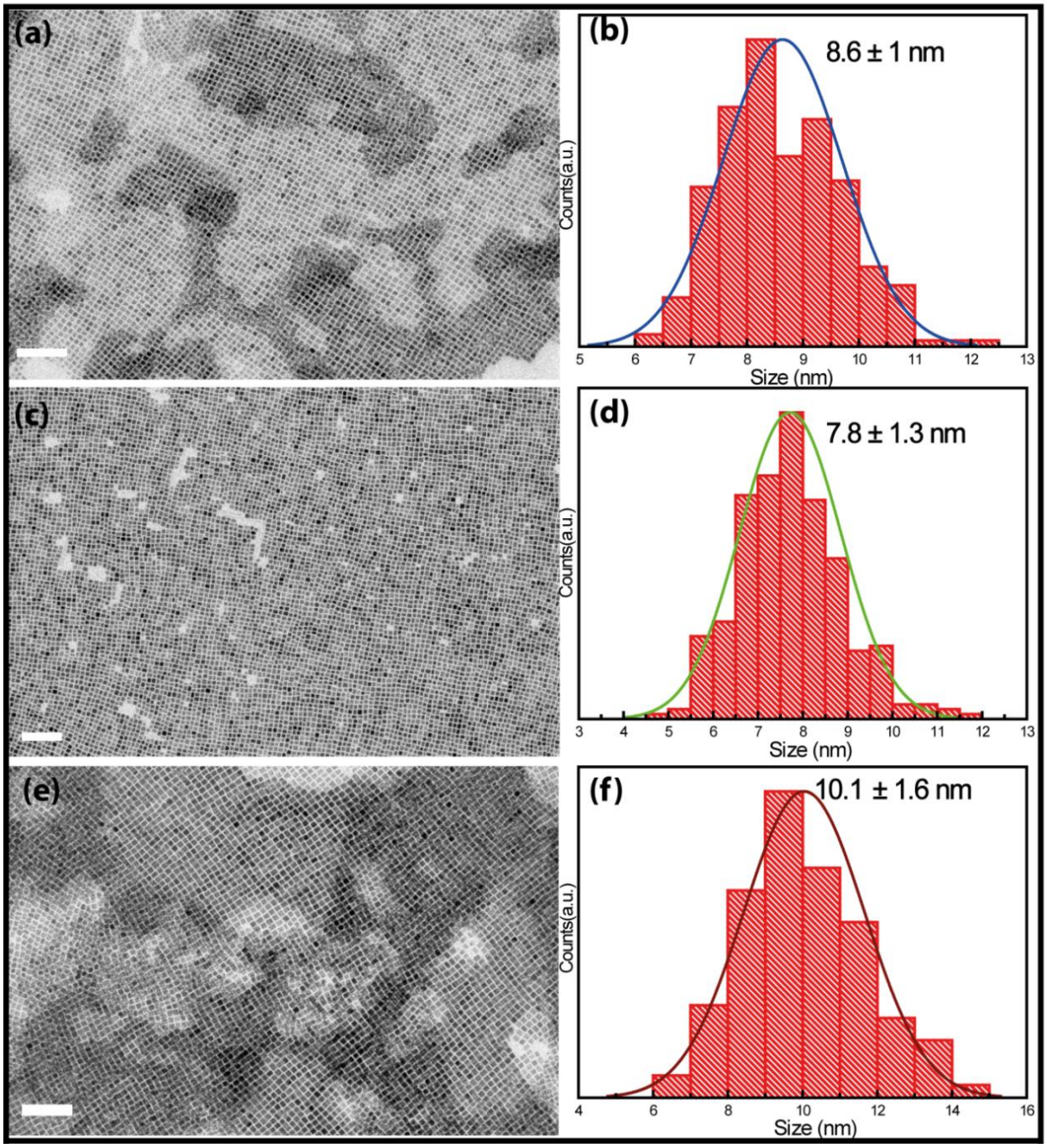

Figure S2. BF-TEM images and size distributions of $CsPbCl_3$ (a, b), $CsPbBr_3$ (c,d), and $CsPbI_3$ (e, f) NCs, respectively. Scale bars are 100nm in all the images.

Time Resolved Spectroscopic Characterization

In order to investigate the photo-physical properties of our $APbX_3$ NCs, we performed Time Correlated Single Photon Counting (TCSPC) measurements. The decay traces at the peak wavelength are shown in Figure S3:

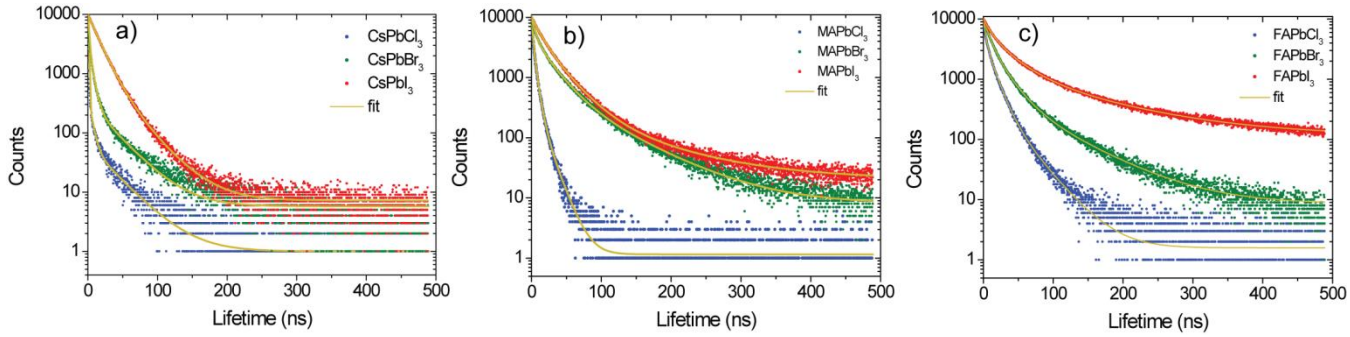

Figure S3. Decay lifetimes of a) $CsPbX_3$, b) $MAPbX_3$ and c) $FAPbX_3$ together with their multi-exponential fittings.

As is commonly observed in perovskite NCs, the decay lifetimes of all the systems show a complex multi-exponential decay trend that has been fitted by means of a three-exponential relation:

$$I(t) = A_1 \cdot e^{\left(\frac{t}{\tau_1}\right)} + A_2 \cdot e^{\left(\frac{t}{\tau_2}\right)} + A_3 \cdot e^{\left(\frac{t}{\tau_3}\right)}$$

in which A_1, A_2 and A_3 are the amplitudes of each of the three components and τ_1, τ_2 and τ_3 are the related time constants. From these values, the average decay lifetime was calculated as follows:

$$\bar{\tau} = \frac{A_1\tau_1^{\,2} + A_2\tau_2^{\,2} + A_3\tau_3^{\,2}}{A_1\tau_1 + A_2\tau_2 + A_3\tau_3}$$

By evaluating the PLQY of all the systems, we were also able to calculate the average radiative and non-radiative recombination rates: with

$$\begin{cases} QY = \dfrac{\Gamma_{rad}}{\Gamma_{rad} + \Gamma_{non-rad}}; \\ \bar{\tau} = \dfrac{1}{\Gamma_{rad} + \Gamma_{non-rad}}; \end{cases}$$

we obtain:

$$\Gamma_{rad} = \frac{QY}{\bar{\tau}}$$

$$\Gamma_{non-rad} = \frac{1}{\bar{\tau}} - \Gamma_{rad} = \frac{(1-QY)}{\bar{\tau}}$$

Table S1. The table encloses all the photo-physical data of all the representative $APbX_3$ NCs.

	A_1	τ_1 (ns)	A_2	τ_2 (ns)	A_3	τ_3 (ns)	τ_{AVG} (ns)	QY %	Γ_{RAD} (1/μs)	$\Gamma_{NON-RAD}$ (1/μs)
$CsPbCl_3$	14471	0.53	418	4.97	60.85	35.44	7.63	65	85.19	45.87
$CsPbBr_3$	6401	1.32	3666	5.05	315.81	34.14	12.52	92	73.45	6.38
$CsPbI_3$	8411	14.43	1686	30.7	16.83	143.31	20.99	58	27.62	20.01
$MAPbCl_3$	4905	1.22	5444	4.24	608	12.39	5.42	5	9.21	175.15
$MAPbBr_3$	4771	5.6	4115	23.91	704	72.02	35	92	26.28	2.28
$MAPbI_3$	4798	12.85	4938	30.08	324	103.01	35.71	45	12.61	15.41
$FAPbCl_3$	4752	2.63	4553	11.88	558	32.13	14.81	2	1.35	66.18
$FAPbBr_3$	4944	8.25	4305	21.06	643	69.37	30.33	92	30.33	2.63
$FAPbI_3$	4329	10.02	4501	36.13	1138	135.01	75.23	55	7.31	5.98

X-ray photoelectron spectra and related quantitative analysis

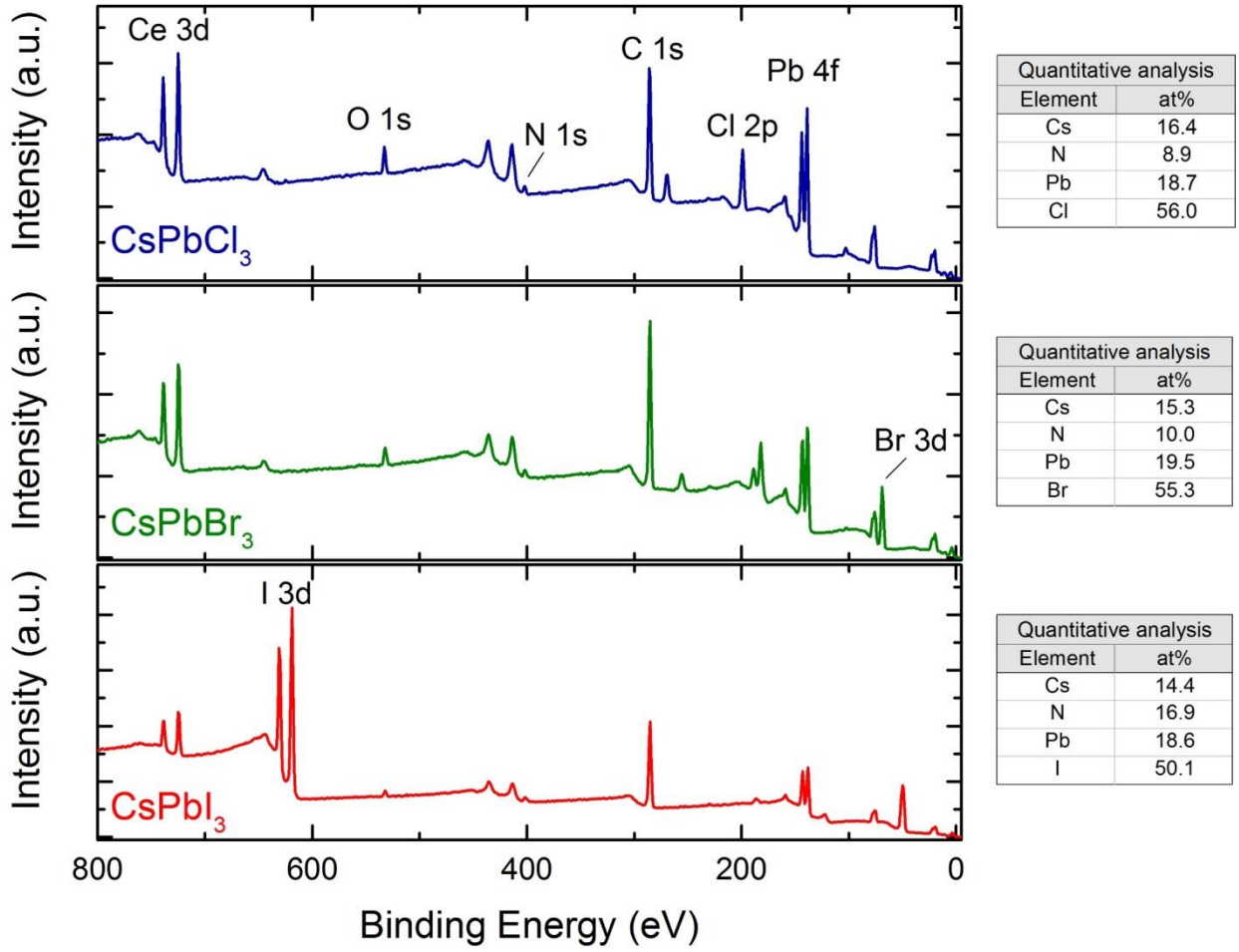

Figure S4. XPS spectra for (A) $CsPbBr_3$, (B) $CsPbCl_3$ and (C) $CsPbI_3$ NCs.

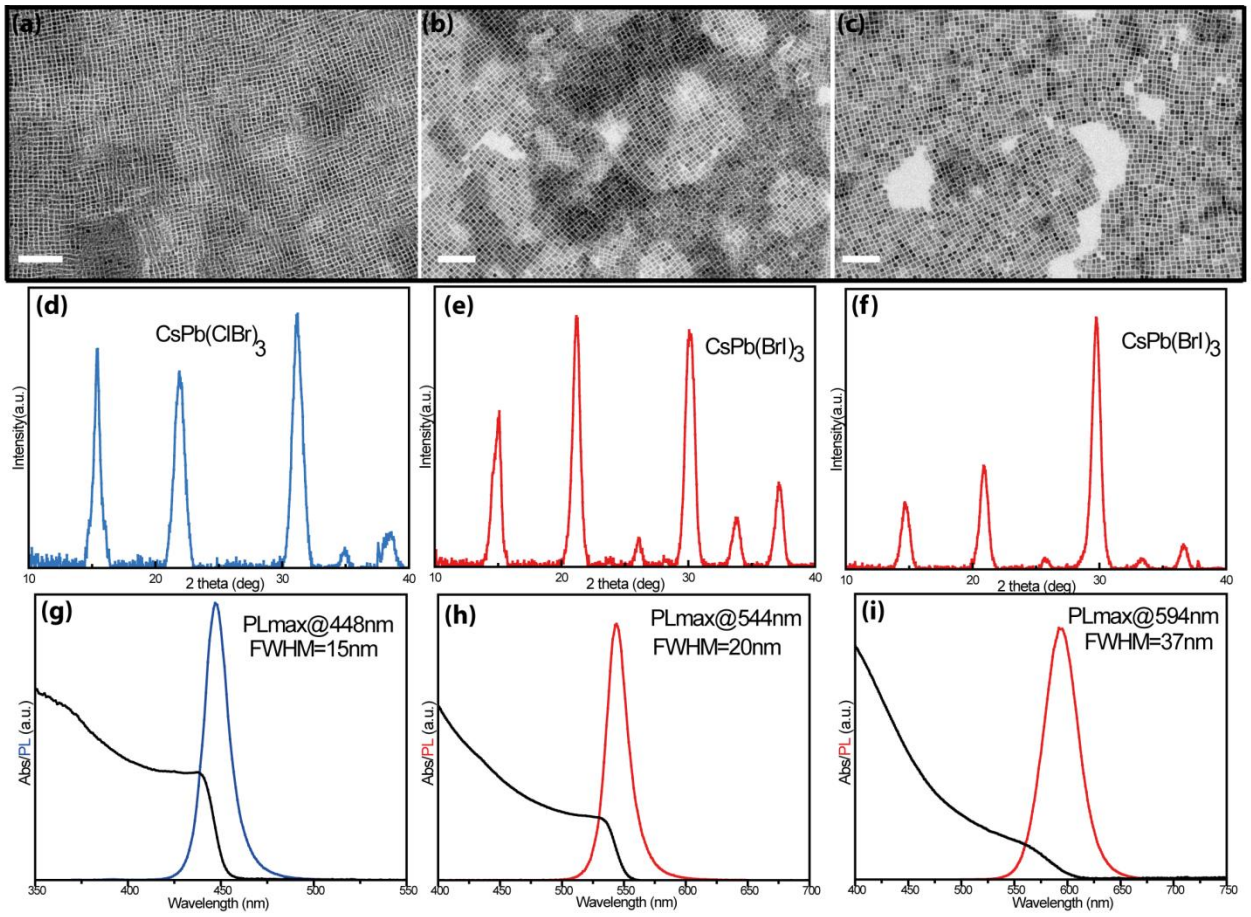

Figure S5. Bright field TEM images of (a) $CsPb(ClBr)_3$ and (b,c) $CsPb(BrI)_3$, NCs. Scale bars are 100 nm in all images. XRD patterns of (d) $CsPb(ClBr)_3$ and (e,f) $CsPb(BrI)_3$ along with their absorption and PL spectra (g-f) respectively.

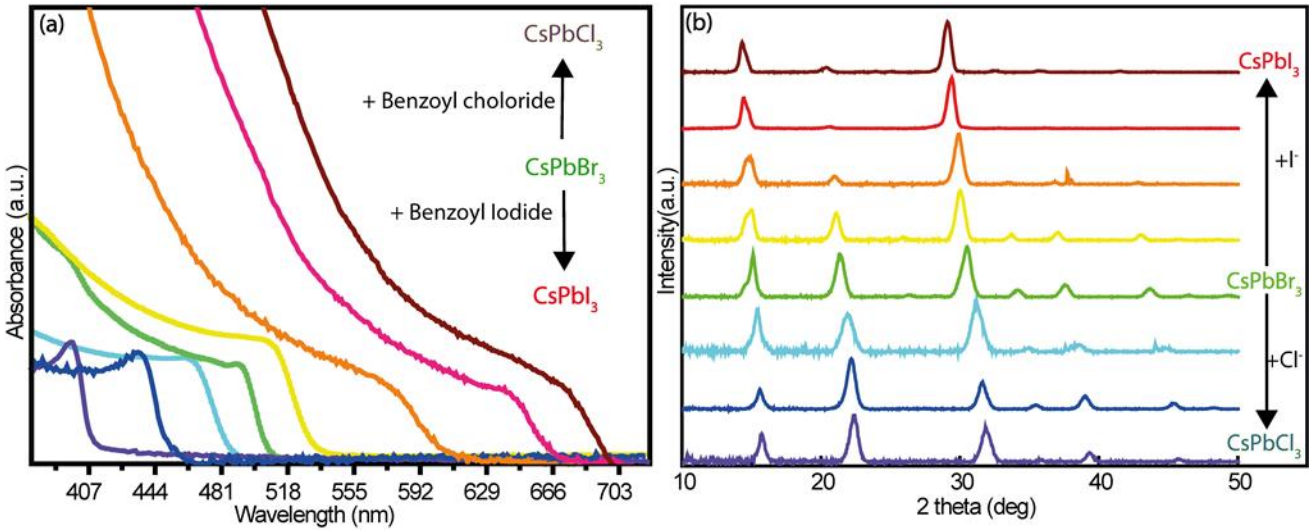

Figure S6. (a) Evolution of the absorbance spectra of representative anion-exchanged NCs, which were obtained from $CsPbBr_3$ NCs by adding benzoyl chloride or benzoyl iodide. (b) XRD patterns of the pristine $CsPbBr_3$ NCs and the anion-exchanged samples (using benzoyl chloride and benzoyl iodide), showing the

retention of the cubic perovskite structure. The shift of the XRD reflections is linearly dependent on the composition, indicating the formation of uniform solid solutions.

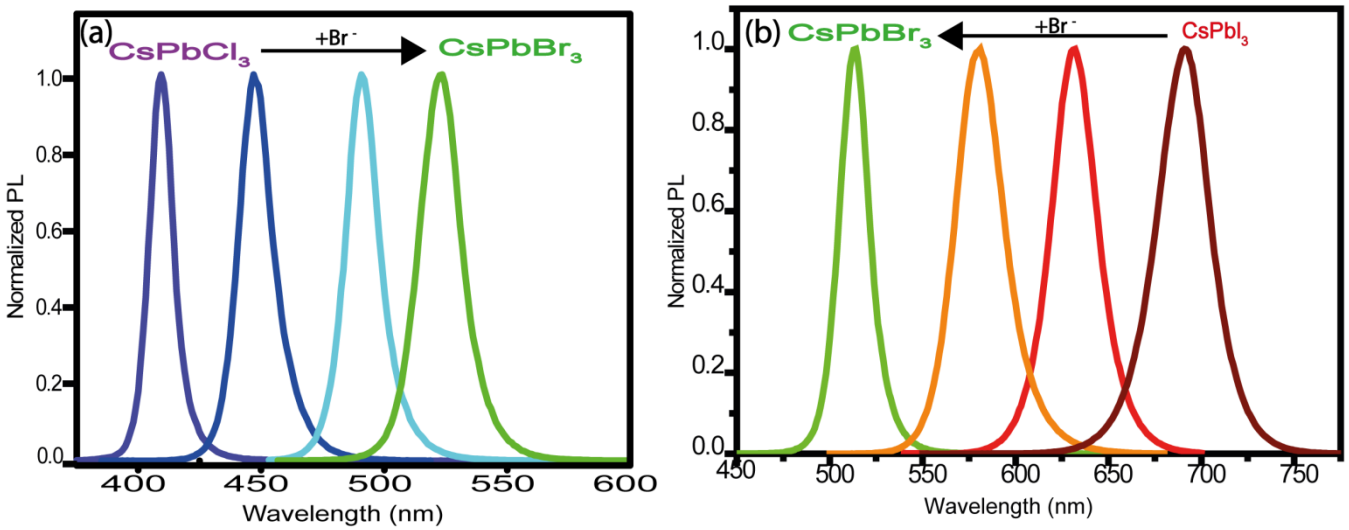

Figure S7. Evolution of the PL spectra of the exchanged NCs that were obtained from $CsPbCl_3$ NCs (upper panel) and $CsPbI_3$ NCs (lower panel) by adding benzoyl bromide.

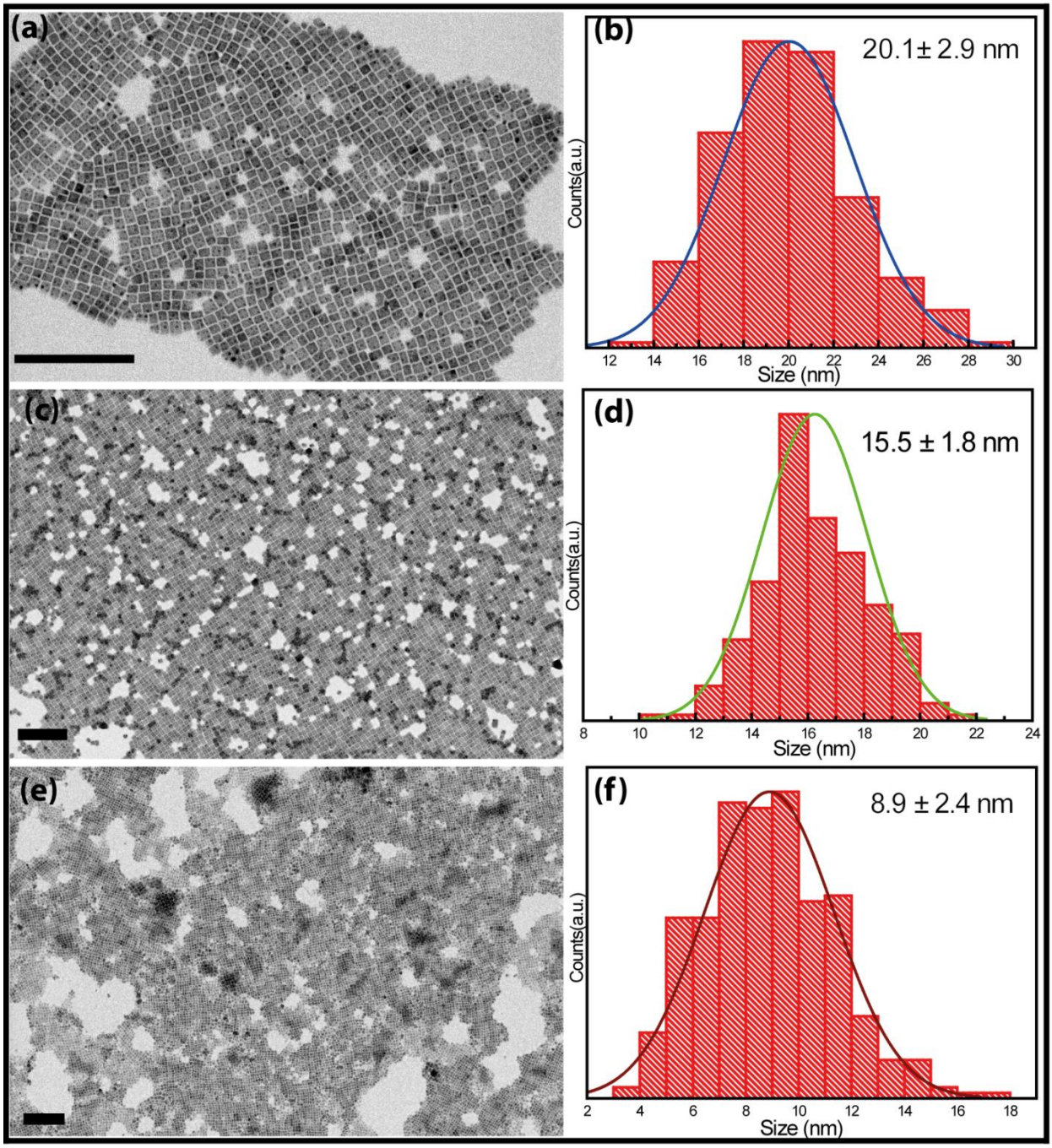

Figure S8. BF-TEM images and size distributions of $MAPbCl_3$ (a, b), $MAPbBr_3$ (c,d), and $MAPbI_3$ (e, f) NCs respectively. Scale bars are 100nm in all the images.

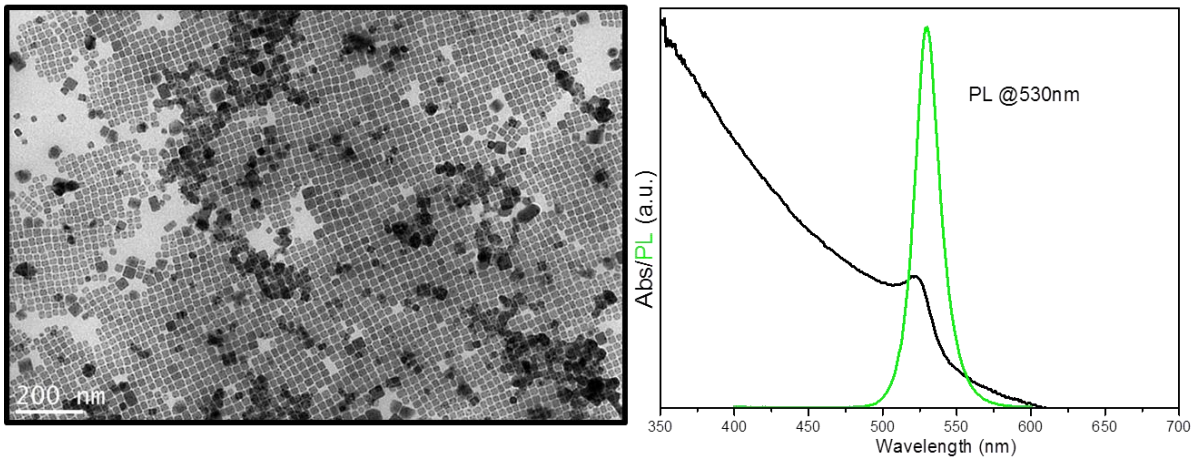

Figure S9. BF-TEM image along with absorption and PL spectra of $MAPbBr_3$ NCs, which were synthesized using lead acetate trihydrate**.**

Control Experiments on $MAPbCl_3$ NCs

We performed the synthesis of $MAPbCl_3$ NCs (as described in the Experimental Details of the main text) increasing the amount of benzoyl chloride from 0.6 to 1.5mmol. The PL emission of the resulting NCs improved when employing 1mmol of the Cl precursor, while poor PL emission was observed when using 1.5mmol of benzoyl chloride (see Figure S4A). The use of 1mmol of benzoyl chloride led also to the formation of a secondary undesired phase: cotunnite $PbCl_2$ (see the Figure below, B panel).

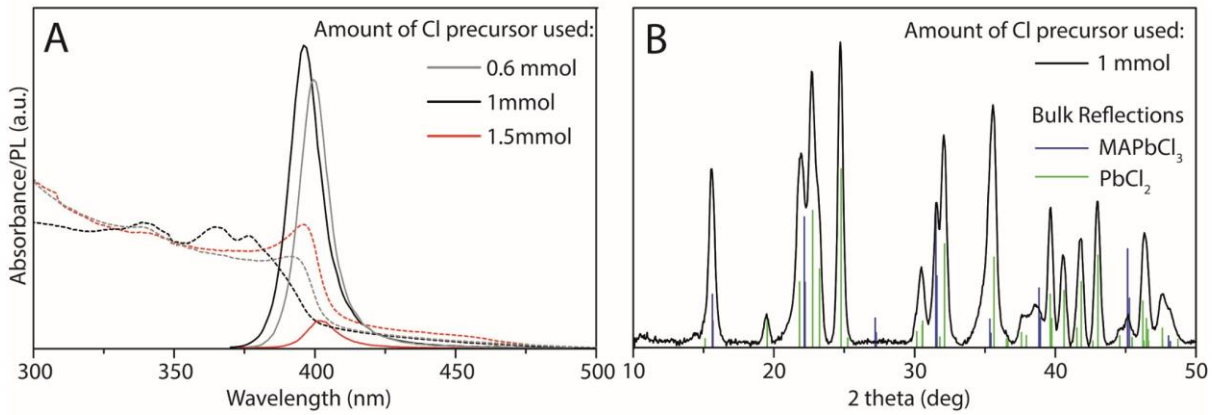

Figure S10. A) Absorption (dashed lines) and PL (solid lines) of $MAPbCl_3$ NCs obtained using 0.6 mmol (gray), 1mmol (black) or 1.5mmol (red) of benzoyl chloride. B) XRD pattern of the $MAPbCl_3$ NCs prepared using 1mmol of benzoyl chloride together with the reference bulk reflections of $MAPbCl_3$ and $PbCl_2$ (ICSD number 2346).

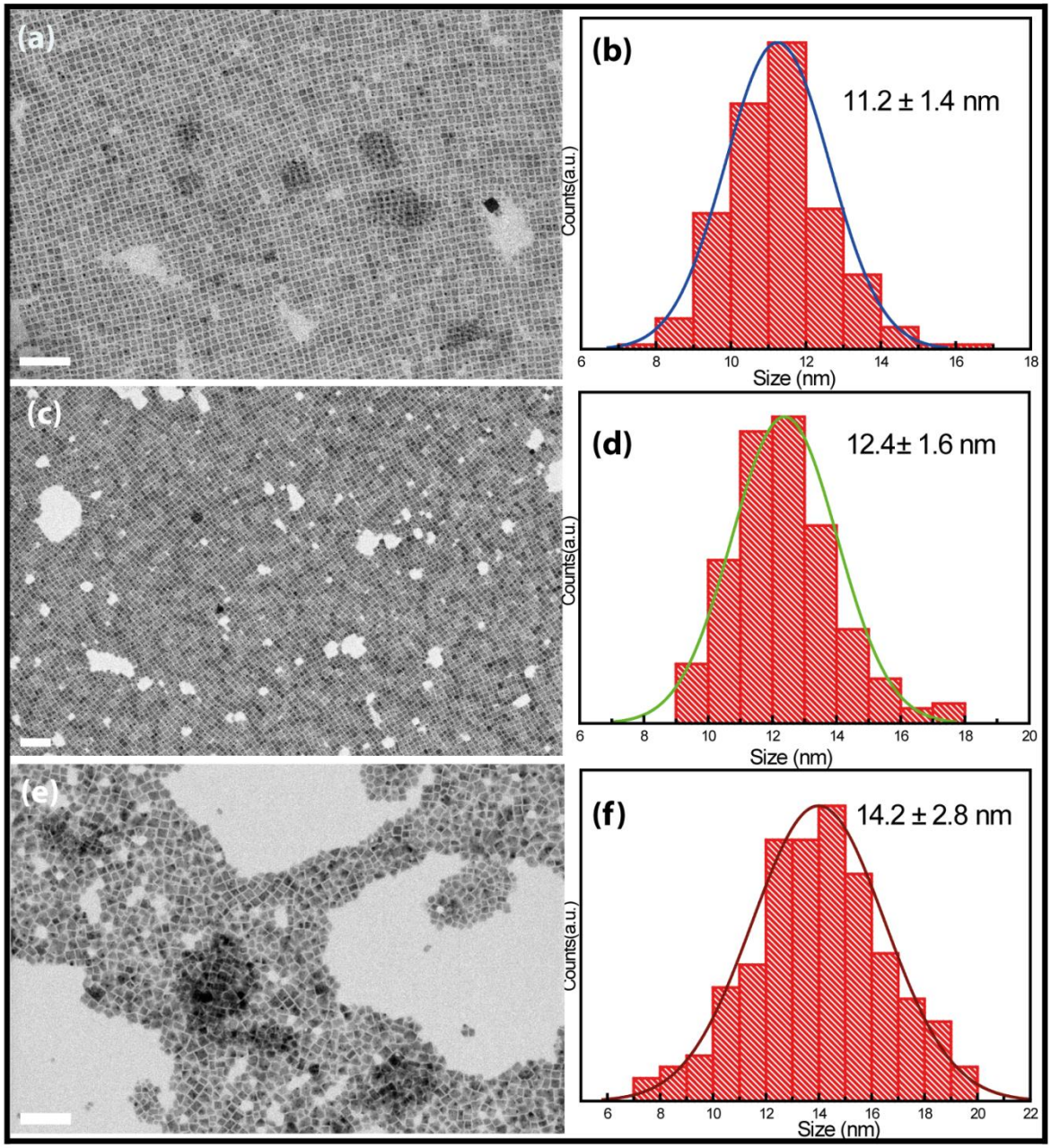

Figure S11. BF-TEM images and size distributions of $FAPbCl_3$ (a, b), $FAPbBr_3$ (c,d), and $FAPbI_3$ (e, f) NCs respectively. Scale bars are 100nm in all the images.

Table S2. Overview of the amplified spontaneous emission thresholds of organic-inorganic and all-inorganic lead bromide perovskite NCs.

Material [morphology]	ASE threshold [μJ/cm²]	Reference
$CsPbBr_3$ [NCs]	2.2	this work
$MAPbBr_3$ [NCs]	4.4	this work
$FAPbBr_3$ [NCs]	8.1	this work
$CsPbBr_3$ [NCs]	5	[2]
$CsPbBr_3$ [NCs]	22	[3]
$CsPbBr_3$ [NCs]	192	[4]
$CsPbBr_3$ [NCs]	2.1	[5]
$MAPbBr_3$ [NCs]	13.9	[6]
$MAPbBr_3$ [NCs]	350	[7]
$MAPbBr_3$ [NWs]	3.0	[8]
$FAPbBr_3$ [NCs]	14	[9]

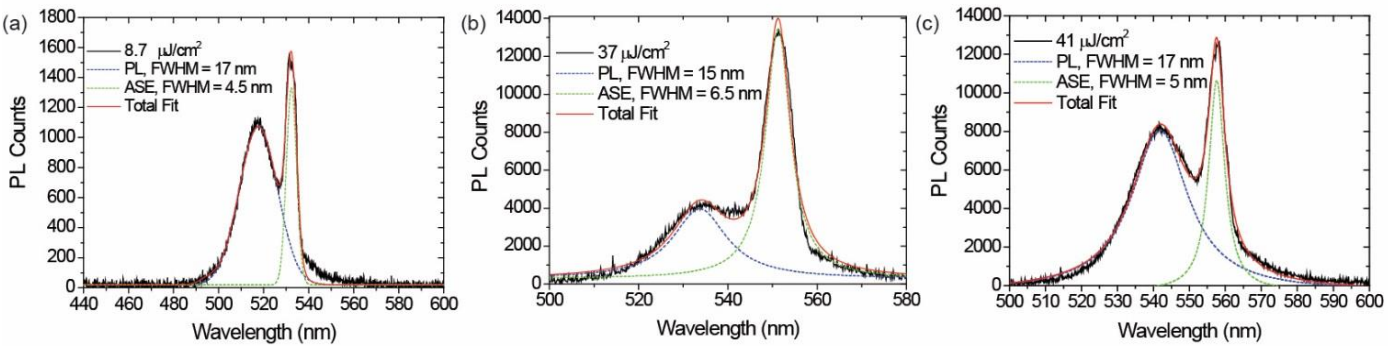

Figure S12. PL and ASE of a) $CsPbBr_3$, b) $MAPbBr_3$ and c) $FAPbBr_3$ systems. The ASE FWHMs were calculated by Lorentizian fitting of the peaks.

Additional references

1. Wu, P. S. C.; Otting, G., Rapid pulse length determination in high-resolution NMR. *J. Magn. Reson.* **2005,** *176* (1), 115-119.
2. Yakunin, S.; Protesescu, L.; Krieg, F.; Bodnarchuk, M. I.; Nedelcu, G.; Humer, M.; De Luca, G.; Fiebig, M.; Heiss, W.; Kovalenko, M. V., Low-threshold amplified spontaneous emission and lasing from colloidal nanocrystals of caesium lead halide perovskites. *Nat. Commun.* **2015,** *6*, 8056.
3. Wang, Y.; Li, X.; Song, J.; Xiao, L.; Zeng, H.; Sun, H., All-Inorganic Colloidal Perovskite Quantum Dots: A New Class of Lasing Materials with Favorable Characteristics. *Adv. Mater.* **2015,** *27* (44), 7101-7108.
4. Pan, J.; Sarmah, S. P.; Murali, B.; Dursun, I.; Peng, W.; Parida, M. R.; Liu, J.; Sinatra, L.; Alyami, N.; Zhao, C.; Alarousu, E.; Ng, T. K.; Ooi, B. S.; Bakr, O. M.; Mohammed, O. F., Air-Stable Surface-Passivated Perovskite Quantum Dots for Ultra-Robust, Single- and Two-Photon-Induced Amplified Spontaneous Emission. *J. Phys. Chem. Lett.* **2015,** *6* (24), 5027-5033.
5. Tong, Y.; Bladt, E.; Aygüler, M. F.; Manzi, A.; Milowska, K. Z.; Hintermayr, V. A.; Docampo, P.; Bals, S.; Urban, A. S.; Polavarapu, L.; Feldmann, J., Highly Luminescent Cesium Lead Halide Perovskite Nanocrystals with Tunable Composition and Thickness by Ultrasonication. *Angew. Chem., Int. Ed.* **2016,** *55* (44), 13887-13892.
6. Veldhuis, S. A.; Tay, Y. K. E.; Bruno, A.; Dintakurti, S. S. H.; Bhaumik, S.; Muduli, S. K.; Li, M.; Mathews, N.; Sum, T. C.; Mhaisalkar, S. G., Benzyl Alcohol-Treated CH3NH3PbBr3 Nanocrystals Exhibiting High Luminescence, Stability, and Ultralow Amplified Spontaneous Emission Thresholds. *Nano Lett.* **2017**, 7424-7432.
7. Priante, D.; Dursun, I.; Alias, M. S.; Shi, D.; Melnikov, V. A.; Ng, T. K.; Mohammed, O. F.; Bakr, O. M.; Ooi, B. S., The recombination mechanisms leading to amplified spontaneous emission at the true-green wavelength in CH3NH3PbBr3 perovskites. *Appl. Phys. Lett.* **2015,** *106* (8), 081902.
8. Vybornyi, O.; Yakunin, S.; Kovalenko, M. V., Polar-solvent-free colloidal synthesis of highly luminescent alkylammonium lead halide perovskite nanocrystals. *Nanoscale* **2016,** *8* (12), 6278-6283.
9. Protesescu, L.; Yakunin, S.; Bodnarchuk, M. I.; Bertolotti, F.; Masciocchi, N.; Guagliardi, A.; Kovalenko, M. V., Monodisperse Formamidinium Lead Bromide Nanocrystals with Bright and Stable Green Photoluminescence. *J. Am. Chem. Soc.* **2016,** *138* (43), 14202-14205.